The Role of Ekman Flow and Planetary Waves in the Oceanic Cross-Equatorial Heat Transport

PAUL S. SCHOPF

Laboratory for Atmospheric Sciences, Goddard Space Flight Center, NASA, Greenbelt, MD 20771

(Manuscript received 2 January 1979, in final form 14 September 1979)

ABSTRACT

A numerical model is used to mechanistically simulate the oceans' seasonal cross-equatorial heat transport, and the results of Oort and Vonder Haar (1976). The basic process of Ekman pumping and drift is found to be able to account for a large amount of the cross-equatorial flux. Increased easterly wind stress in the winter hemisphere causes Ekman surface drift poleward, while decreased easterly stress allows a reduction in the poleward drift in the summer hemisphere. When the annual mean flow is removed, a net flow at the surface from summer to winter hemispheres is noted. The addition of planetary and gravity waves to this model does not alter the net cross-equatorial flow, although the planetary waves are clearly seen. On comparison with Oort and Vonder Haar (1976), this adiabatic advective redistribution of heat is seen to be plausible up to 10–20°N, beyond which other dynamics and thermodynamics are indicated.

1. Introduction

This paper is an initial report on an investigation of how the ocean acts to transport heat across the equator on a seasonal time scale. The study of this question was undertaken upon viewing the results of Oort and Vonder Haar (1976) for the ocean heat transport as a function of time. They showed evidence that there was a large ($\sim 4 \times 10^{15}$ W) annual cycle of heat transport in the oceans at low latitude. This oscillation dominates the ocean behavior at low latitudes, almost completely masking the annual mean. Up to 20°N, the ocean heat transport changes direction at some time during the year, with heat apparently flowing from the summer to winter hemisphere. It was felt that with such a large magnitude, mechanisms for this transport should be readily identifiable, and it was hoped that some fairly simple models for the ocean behavior could account for this heat transport. This first report describes the results of a study of a linear, adiabatic ocean circulation with variable wind driving.

Several investigators have recently studied the response of the tropical ocean to applied winds (McCreary, 1976; Cane and Sarachik, 1976, 1977; Moore and Philander, 1977; among others). They have provided a rich description of the many interesting wave phenomena involved in the spin-up problem or response to abnormal winds.

The waves of particular interest are the planetary (Rossby) waves and the gravity waves. The Kelvin and Yanai (mixed Rossby-gravity) waves also arise, although they are strongly trapped at the equator. The model studied here allows for the propagation of these waves, together with direct Ekman circulation. While restricting the solutions to linear waves without heat exchange across the surface, the propagation of the waves is modeled using finite differences, avoiding the problems associated with changing wavenumbers and group velocity. It is noted that significant north-south group velocity will be introduced into waves propagating out from a meridional wall (Schopf *et al.*, 1980).

The question to be answered is whether the existence of the planetary waves significantly alters the expected response to Ekman pumping. Meyers (1975) has shown some evidence to support the notion that direct Ekman pumping may cause thermocline displacement. By inference, this must mean that direct Ekman flow is converging the warm surface waters over the area where the thermocline is deepening and, therefore, it must collect heat. The results of White (1977) and McCreary (1976), however, show the possibility that planetary waves could alter the picture seen by Meyers.

If one views the problem in the terms used by McCreary (1976), the complex current structure can be viewed as a zonally uniform "interior" flow plus a series of propagating waves. The interior solution is a particular solution to the set of equations with forcing but without meridional boundaries. Free wave solutions are then superposed to satisfy boundary conditions.

This distinction between a response which does not feel the effects of the boundaries and another propagating component has been discussed by

Anderson and Gill (1975) in connection with the spin-up to Sverdrup flow of a midlatitude ocean. When the winds vary in a cyclic fashion, the establishment of the Sverdrup regime is modified to become a series of planetary waves with a period equal to that of the forcing—provided, of course, that the wavelength at this period is somewhat less than the basin width.

In a model without a western boundary, and with adiabatic advection as the heat transfer mechanism, the planetary waves will carry no net heat poleward. Alternating northward and southward moving sectors will cancel each other. Once a western boundary is imposed, however, the net transport due to the oscillating waves need not be zero. This is particularly true where the half-wavelength of the wave is approximately the width of the basin.

The model constructed here allows for the excitation of these planetary waves within a simple bounded ocean. It consists of a wind-driven current model with a specified mean thermal and density structure dependent only on depth about which the response is linearized. Heat is transported in this model by net meridional overturning. As such, it is the zonal mean meridional velocity field which is important to the heat transport. Calculation is facilitated by decomposing the variables into vertical normal modes. For all modes other than the barotropic, the net flow throughout any one column is zero. Whatever flow is poleward near the surface must be fully returned at some lower depth. Thus a given value of modal velocity actually represents a certain amount of overturning with a particular vertical structure. If the vertical thermal structure is known, then

$$\text{Heat Transport} = \rho c_p \int_{-H}^{0} v(z)T(z)dz. \quad (1.1)$$

If

$$v(z) = \sum_n v^n P^n(z), \quad (1.2)$$

where P^n is the eigenfunction for the vertical structure, then

$$\text{Heat Transport} = \sum_n v^n \left[\rho c_p \int_{-H}^{0} P^n(z)T(z)dz \right]. \quad (1.3)$$

Note that the term in brackets on the right-hand side of (1.3) is a function of the known temperature and eigenfunctions. It may be computed before solutions for v^n, and thus

$$\text{Heat Transport} = \sum_n v^n S^n, \quad (1.4)$$

where S^n is the bracketed quantity in (1.3).

Hellerman (1977, personal communication) has added many new wind roses and pilot chart information to the data base used in his 1967–68 estimate of global wind stresses. This has allowed global estimates on a monthly basis for 2.5° × 2.5° grids. From these data, zonal means of the stress components were analyzed to determine the phase and amplitude of the annual cycle. Fig. 1.1 shows the cycle of mean zonal wind stress as a function of latitude, which is of primary interest for this study.

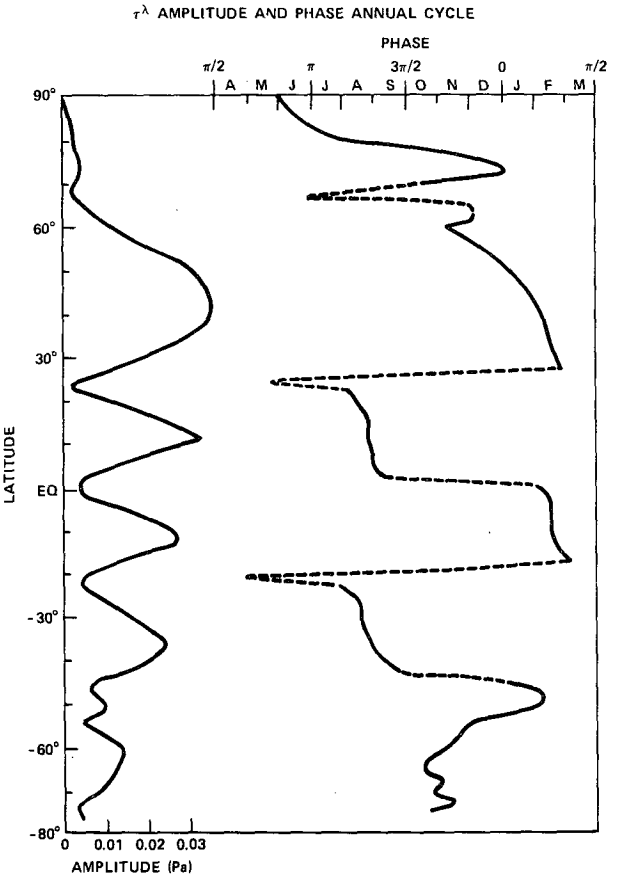

FIG. 1.1. Zonal mean westerly wind stress, annual cycle (from Hellerman, 1977, personal communication). Phase is relative to 1 January for a cosine transform.

A strengthening of low-latitude easterlies is seen in both hemispheres during their winter months. This field is approximated by

$$\tau_1^\lambda/\rho_0 = -3 \times 10^{-5} \sin(180\theta/22) \cos(\sigma t) \ [\text{m}^2\ \text{s}^{-2}], \quad (1.6)$$

where τ_1^λ is the amplitude of the zonal stress, ρ_0 is the mean density of the ocean, $\sigma = 2\pi/1$ year and θ is latitude.

Meridional winds drive meridional velocities only very near the equator, where ageostrophic effects become important. As such, the details of the meridional wind field outside of the latitude band of 5°S to 5°N are unimportant. Within this region, the annual cycle in meridional stress is quite uniform and has an amplitude of about 0.2 dyn cm^{-2}. It will be seen that the response to meridional winds is of

TABLE 2.1. Mean density and thermal data.

Z (m)	$\rho - 1$ (10^{-3} g cm^{-3})	T (°C)
25	23.2	26.2
75	23.3	24.2
125	24.0	21.6
200	25.9	17.3
300	26.7	12.7
425	26.9	9.6
575	27.1	7.2
725	27.3	5.8
900	27.45	4.8
1125	27.6	3.9
1375	27.75	3.0
1625	27.85	2.5
1875	27.925	2.1
2125	28.0	1.9
2375	28.05	1.8
2750	28.10	1.6
3250	28.27	1.5
3750	28.33	1.5
4250	28.385	1.4
4750	28.435	1.3

secondary importance for the cross-equatorial heat transport, so a detailed description of the wind field need not be made.

2. A linear model of the seasonal response

By decomposing variables into vertical normal modes, equations for linear, hydrostatic Boussinesq flow on the sphere may be written in terms of u^n, v^n and p^n, the modal velocities and pressure. Following the procedure outlined in Moore and Philander (1977), for example, but retaining spherical coordinates, the modal equations are

$$\partial u^n/\partial t - fv^n + (1/\rho_0 a \cos\theta)\partial p^n/\partial\lambda = b^{\lambda n}, \quad (2.1a)$$

$$\partial v^n/\partial t + fu^n + (1/\rho_0 a)\partial p^n/\partial\theta = b^{\theta n}, \quad (2.1b)$$

$$\partial p^n/\partial t + (gh^n/a)\cos\theta[\partial u^n/\partial\lambda + \partial(v^n\cos\theta)/\partial\theta] = 0, \quad (2.1c)$$

where θ and λ are the latitude and longitude, a is the radius of the earth and

$$(u,v,p,b) = \sum_n (u^n,v^n,p^n,b^n)P^n(z), \quad (2.2)$$

where $P^n(z)$ are the eigenfunctions of the vertical separation equation and h^n is the equivalent depth. Calculation of the eigenfunctions and vertical thermal structure was based on data for the Pacific analyzed by Levitus and Oort (1977). The Brunt-Väisälä frequency was computed from the zonal mean density fields between 30°N and 30°S, as given in Table 2.1. The wind stresses b^λ and b^θ are treated as body forces distributed over a mixed layer of depth d, i.e.,

$$b^{(\lambda,\theta)} = \frac{1}{\rho_0}\frac{\partial\tau^{(\lambda,\theta)}}{\partial z} = \begin{cases}\tau(0)^{(\lambda,\theta)}/\rho_0 d, & -d \le z < 0 \\ 0, & -H < z < -d.\end{cases} \quad (2.3)$$

For each mode b^n is proportional to $\tau(0)$:

$$b^n = \frac{1}{H}\int_{-H}^{0} b(z)P^n(z)dz, \quad (2.4a)$$

$$b^n = \frac{(\tau(0)/\rho)}{H}\int_{-d}^{0} P^n/ddz, \quad (2.4b)$$

$$b^n = \tau(0)B^n/\rho_0. \quad (2.4c)$$

For the first 12 vertical modes, Table 2.2 lists the equivalent depth B^n as defined by (2.4) and S^n as defined in (1.4).

Solutions to (2.1a–c) contain the interior flow, plus gravity, planetary, Kelvin and Yanai waves. It is these equations (or their β-plane equivalents) which have been recently subject to a large amount of investigation. Here, it is the behavior of solutions at very low frequencies which are of interest.

At the outset, several points can be noted. At a frequency of $2\pi/(1\text{ year})$, gravity waves do not enter explicitly, the Yanai wave is approximately a nondivergent short Rossby wave, and the Kelvin wave has a wavelength of over 10^5 km.

If the forcing is independent of λ, then the interior solutions are also λ independent. Dropping the modal superscript n, and writing

$$v_i = \tilde{v}_i \exp(-i\sigma t), \quad (2.5)$$

a single equation for $\tilde{v}_i$ is given by

$$(\sigma^2 - f^2)\tilde{v}_i + \frac{gh}{a^2}\frac{\partial}{\partial\theta}\left[\frac{1}{\cos\theta}\frac{\partial}{\partial\theta}(\tilde{v}_i\cos\theta)\right] = f\tilde{b}^\lambda - i\sigma\tilde{b}^\theta, \quad (2.6)$$

TABLE 2.2. Modal properties.

Mode	h^n (m)	B^n (m^{-1})	S^n (10^7 J m^{-2})
0	5000.	0.0073	0
1	1.00	0.0508	136.95
2	0.40	0.0535	45.05
3	0.17	0.0235	−11.12
4	0.079	0.0172	−10.12
5	0.051	0.0158	−2.81
6	0.037	0.0106	−1.43
7	0.029	0.0071	3.65
8	0.022	0.0047	5.26
9	0.018	0.0020	4.18
10	0.015	−0.0004	0.92
11	0.013	−0.0014	0.78
12	0.011	−0.0038	−1.19

from which the small response to b^θ relative to b^λ is deduced since $\sigma \ll f$ except within a few kilometers of the equator.

a. Zonal winds

For the large-scale forcing described by (1.6), the dominant balance for $n > 0$ is given by

$$f\tilde{v} = -\tilde{b}^\lambda, \tag{2.7}$$

which is just the Ekman layer response as cast in terms of the vertical modes. For the particular choice of b^λ due to (1.6), the right-hand side of (2.6) remains well-behaved at the equator. Since modal amplitudes of $\tilde{v}$ are directly proportional to the amplitude of $\tilde{b}^\lambda$, upon resynthesis, the vertical shape of v will be the same as that chosen for $b(z)$.

Full solutions to (2.6) can be obtained by replacing derivatives with finite differences and solving the resultant tri-diagonal matrix problem. Solutions for modes 0, 1 and 2, with $b^\theta = 0$ are shown in Fig. 2.1, together with the Ekman approximation for mode 1. The Ekman approximation is seen to hold very closely for the higher modes. The barotropic mode, however, shows the influence of the second term in (2.6).

Upon resynthesis of $v(z)$ from the modal solutions to (2.6), it will be found that, except for some uniform barotropic flow, the velocity field does in fact mirror the vertical structure of the applied forcing field. A uniform meridional flow is seen for $-d < z < 0$, with incomplete return flow below $-d$.

Returning to the question of heat transport, if the barotropic mode is neglected, the heat transport by the sum of solutions to (2.6) should closely approximate that found from Ekman layer circulation alone. Fig. 2.2 shows heat transport versus time for the Ekman approximation and for the sum of the first 12 interior solutions to (2.6) with $b^\theta = 0$. The agreement is indeed very good.

b. Meridional winds

For meridional winds the response is strongly trapped near the equator. Solutions to (2.6) with

$$\tau^\theta(0)/\rho_0 = 3 \times 10^{-5} \sin(\sigma t) \tag{2.8}$$

were computed. Response of the first two modes is shown in Fig. 2.3, together with results from Fig. 2.2. The solutions are strongly trapped near the equator, and smaller by a factor of 10 or more than solutions with zonal forcing. Different shapes for b^θ do not significantly change the character of the response. Succeeding discussion therefore will neglect the effect of meridional winds.

3. Wave solutions

Solutions to (2.1a–c), with $\sigma \ll f$ are approximated by

$$-fv_i = b^\lambda, \tag{3.1}$$

$$\partial u_i/\partial t = -\frac{gh}{\rho_0 a^2 f}\frac{\partial}{\partial\theta}\left[\frac{1}{\cos\theta}\frac{\partial}{\partial\theta}\left(\frac{b}{f}\right)\right], \tag{3.2}$$

where u_i is independent of λ. These solutions violate the boundary conditions required by rigid walls at the eastern and western ends of the basin, i.e., $u = 0$ at $\lambda = 0, L$. This inconsistency is solved by the generation of waves from the walls such that

$$u_w(0,\theta,t) = -u_i(0,\theta,t), \tag{3.3a}$$

$$u_w(L,\theta,t) = -u_i(L,\theta,t). \tag{3.3b}$$

These waves propagate freely about the basin, and alter the character of the response.

The waves present at $\sigma = 2\pi/(1\text{ year})$ are the long westward propagating Rossby waves, the short eastward propagating Rossby waves and an equatorially trapped Kelvin wave.

In order to determine the effects of the waves on the net heat transport, a numerical model was used to solve (2.1a–c) with some dissipation added. A biharmonic damping was added to minimize the dissipation of the longer waves while still allowing control of the narrow western boundary currents.

The equations to be solved become

$$\frac{\partial u}{\partial t} - fv + \frac{1}{\rho_0 a\cos\theta}\frac{\partial p}{\partial\lambda} = b^\lambda - B_m\nabla^2\nabla^2 u, \tag{3.4a}$$

$$\frac{\partial v}{\partial t} + fu + \frac{1}{\rho_0 a}\frac{\partial p}{\partial\theta} = b^\theta - B_m\nabla^2\nabla^2 v, \tag{3.4b}$$

$$\frac{\partial p}{\partial t} + \frac{\rho_0 gh}{a\cos\theta}\left[\frac{\partial u}{\partial\lambda} + \frac{\partial}{\partial\theta}(v\cos\theta)\right] = 0. \tag{3.4c}$$

Extra boundary conditions are needed with the biharmonic friction, so the free-slip conditions are extended to

$$u = 0, \quad \frac{\partial v}{\partial\lambda} = 0, \quad \frac{\partial^2 v}{\partial\lambda^2} = 0,$$

at

$$\lambda = 0,\ 100°\text{E}, \tag{3.5a}$$

$$v = 0, \quad \frac{\partial u}{\partial\lambda} = 0, \quad \frac{\partial^2 u}{\partial\lambda^2} = 0, \quad \text{at} \quad \theta = 50°\text{N}, \tag{3.5b}$$

$$\frac{\partial v}{\partial\theta} = 0, \quad u \text{ antisymmetric}, \quad \text{at} \quad \theta = 0, \tag{3.5c}$$

where the symmetry of the equations are employed to reflect the solutions about the equator. With b^λ antisymmetric, v is symmetric and u and p are antisymmetric.

a. The first baroclinic mode

The model was run to 5.0 years with $B_m = 1.25 \times 10^{22}$ cm^4 s^{-2}. On the 1° grid, the decay time for the shortest wave resolved is equivalent to that for Laplacian friction ($A_m \nabla^2 u$) with $A_m = 10^9$ cm^2 s^{-1}.

Fig. 3.1 shows the instantaneous pressure field associated with the first mode at $t = 5.0$ years.

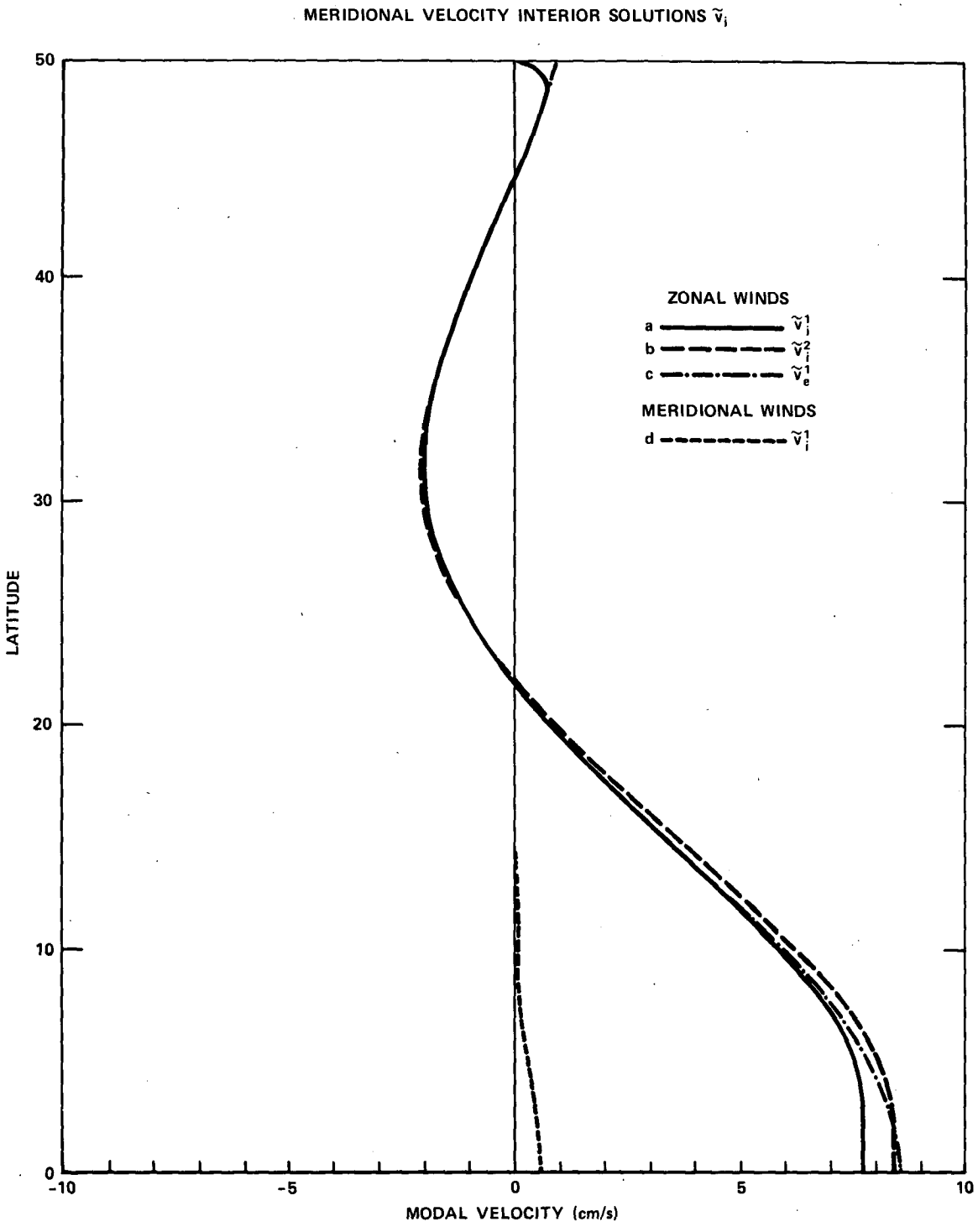

FIG. 2.1. Interior solutions for meridional velocity: (a) solution to (2.7) with zonal winds, first baroclinic mode; (b) solution to (2.7) with zonal winds, second baroclinic mode; (c) Ekman approximation (2.8) with zonal winds, first baroclinic mode; (d) interior solution to (2.7) with meridional winds. Zonal winds given by (1.6), meridional winds by (2.9).

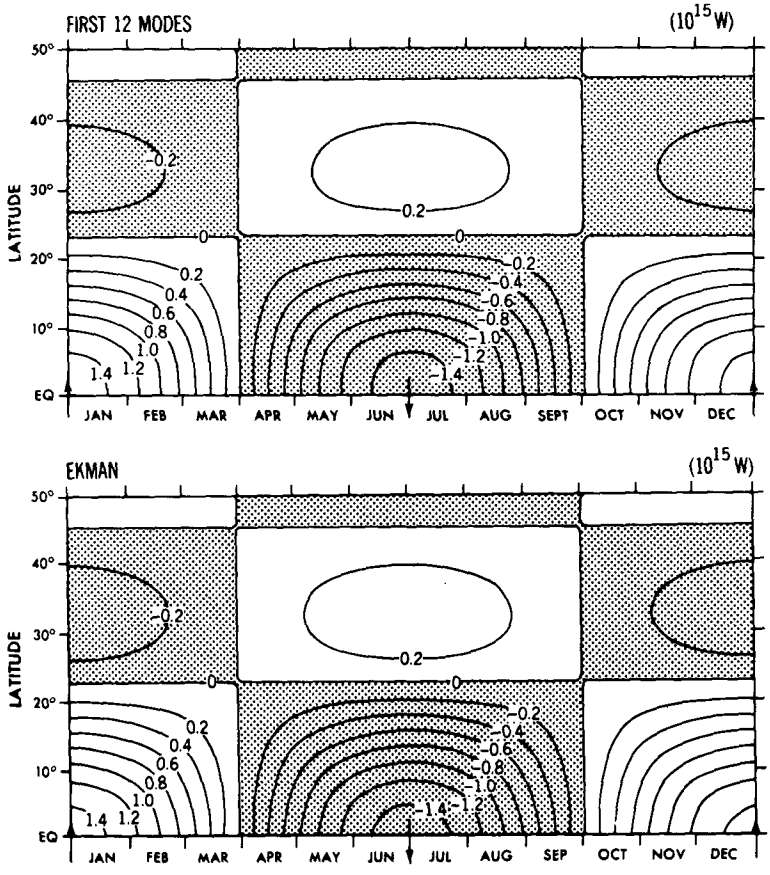

FIG. 2.2. Heat transport over a 100° basin versus time for interior solutions, zonal winds: (a) Ekman approximation, (b) sum of first solutions to (2.7) for first 12 baroclinic modes.

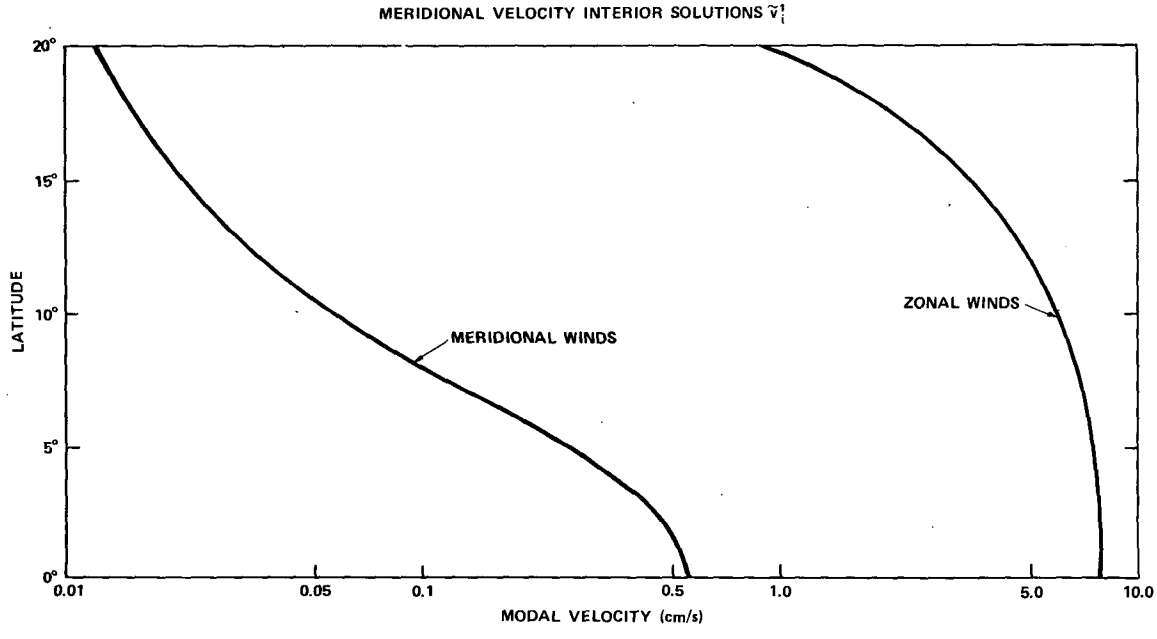

FIG. 2.3. Interior solutions to (2.7) for zonal winds and meridional winds on logarithmic scale for 20°.

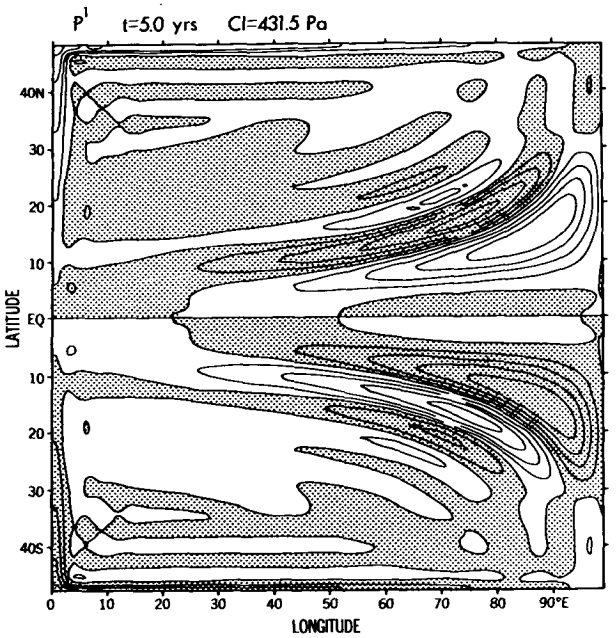

FIG. 3.1. Pressure field for first baroclinic mode at $t = 5.0$ years from the finite difference solution of (3.4a–c) on a 1° grid. Model was started from rest at $t = 0$, and forced by wind stress according to (1.6).

This pressure field is a measure of the thermocline displacement and so shows the effect of the waves and the Ekman flow on heat storage. The time shown corresponds to Northern Hemisphere winter, with the amplitude of the wind stress at its maximum. Fig. 3.2 shows the corresponding map of meridional velocity.

The Rossby waves propagating from the eastern boundary are clearly seen to have a strong impact on the local structure of the thermocline. However, in the velocity field, the tendency for a zonally uniform Ekman response is equally apparent. Since the quantity of interest is the zonally integrated heat transport, it is the mean meridional velocity which must be considered. For the full λ-dependent solutions, Eq. (1.4) remains valid if v is allowed to vary in λ:

$$HT^n(\theta,t) = S^n \int_0^{\Delta\lambda} v^n(\lambda,\theta,t) a \cos\theta d\lambda. \quad (3.6)$$

For comparison with the results of Section 2, it is noted that the interior solutions transport heat over a finite basin width by the relation

$$HT_i^n = S^n v_i^n \Delta\lambda a \cos\theta, \quad (3.7)$$

where $\Delta\lambda$ is the basin width. Fig. 3.3 shows HT_i^1 and HT^1 for one annual cycle (4.0–5.0 years for HT^1). Although there is some distortion of the patterns, both the general structure and amplitudes are remarkably close. This implies that the free waves excited at the boundaries have no net transport when integrated across the basin. While they may affect the local response in very important ways, they do not get rectified by the presence of a western wall, even very close to the equator, where the free wavelength, in fact, is much longer than the basin width.

b. The second baroclinic mode

Considering the slower wave speeds for the second baroclinic mode, it is expected that the western propagating long waves will show more cycles across the basin. The "free" wave behavior—as indicated by a lack of strong interaction with the western boundary—will extend further south than that for the first baroclinic mode. This will imply greater agreement between $\bar{v}^{(2)}$ and $v_i^{(2)}$, since it is only through interaction with the western boundary that significant rectification can occur.

Fig. 3.4 supports these predictions. The pattern of $v^{(2)}$ at $t = 3.0$ years is shown. Shorter wavelengths and less propagation are seen, especially north of 15°.

c. The barotropic mode

The barotropic mode presents somewhat of a difficulty for the analysis of heat transport. Since there is a net flux of mass across any latitude belt, there must be a flux of heat, since the column possesses thermal energy. However, for the purposes of air-sea interaction, the accumulation of

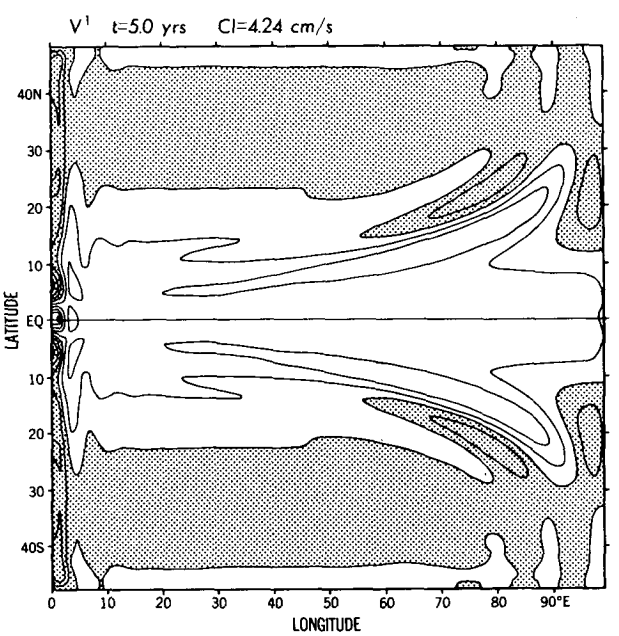

FIG. 3.2. Meridional velocity field for first baroclinic mode at $t = 5.0$ years.

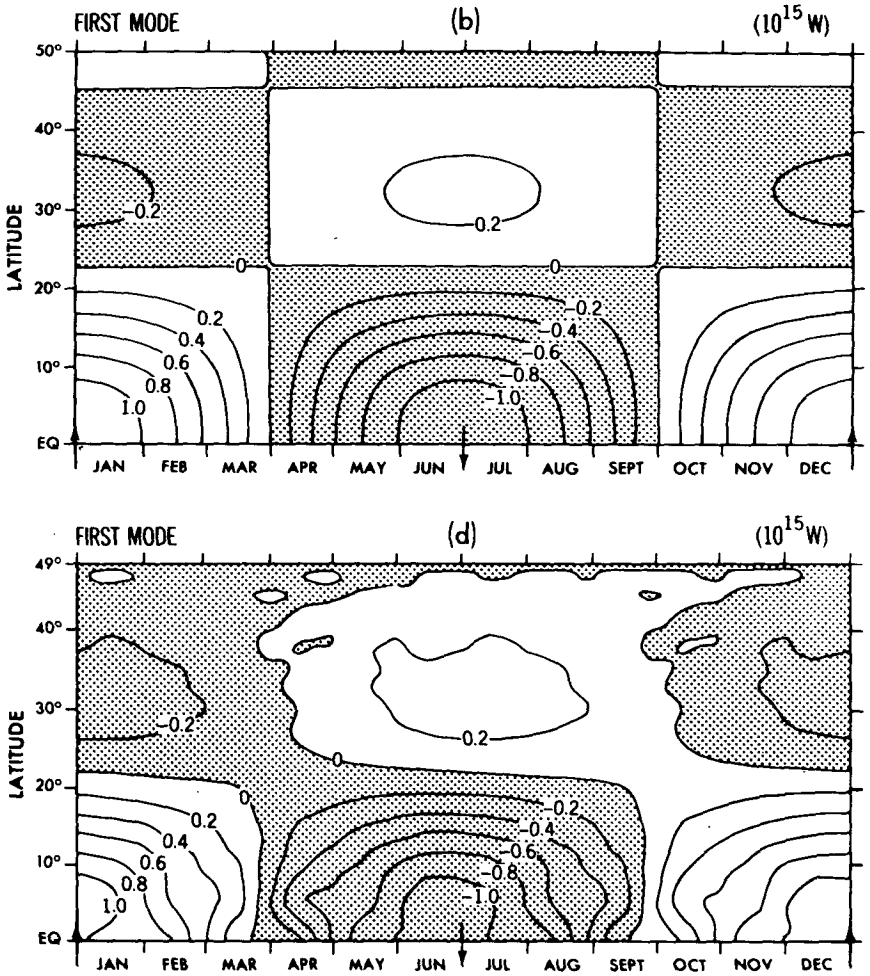

FIG. 3.3. Northward heat transport over a 100° basin versus time by first baroclinic mode components of (a) interior solutions to (2.6), and (b) finite difference solutions of (3.4a–c).

mass (and thereby heat) in the abyssal ocean is not of interest. Rather, it is appropriate to ask how the barotropic motion affects heat storage in the upper ocean, where thermodynamic interaction with the surface can occur.

This influence of storage is given by the fraction of total barotropic mass convergence which occurs in the upper ocean. That is, if the surface of a 5000 m deep ocean is displaced 5 cm by barotropic convergence, the thickness of the top 100 m will be increased by 1 mm.

Numerical simulation of the barotropic mode reveals two relevant points. Fig. 3.5 shows the barotropic pressure field at $t = 12$ days. As expected, the high Rossby wave speed allows for the development of a Sverdrup regime within a very short time. In addition, the surface displacements associated with the barotropic mode are on the order of 10 cm. Therefore, the influences of the barotropic motion on the heat storage cycle may safely be neglected.

4. Discussion

The results of this study of the wind-driven seasonal ocean circulation point to the importance of the direct Ekman effect on the zonally averaged heat transport. Although the long planetary waves strongly modify the local behavior, they are unable to seriously affect the overall heat balance. The picture which emerges is one of Ekman convergence in the winter hemisphere and divergence in the summer hemisphere, providing a shallowing and deepening of the mixed layer, against the effects of local heating. While the Coriolis force vanishes at the equator, continuity and direct pressure driven flow complete the Ekman flow pattern across the equator.

This picture agrees superficially with the results of Meyers (1975), where he showed correlation between depth of the thermocline and Ekman convergence. However, since Meyers' work covered a limited area, it would be more appropriate to compare the depth of the thermocline (approxi-

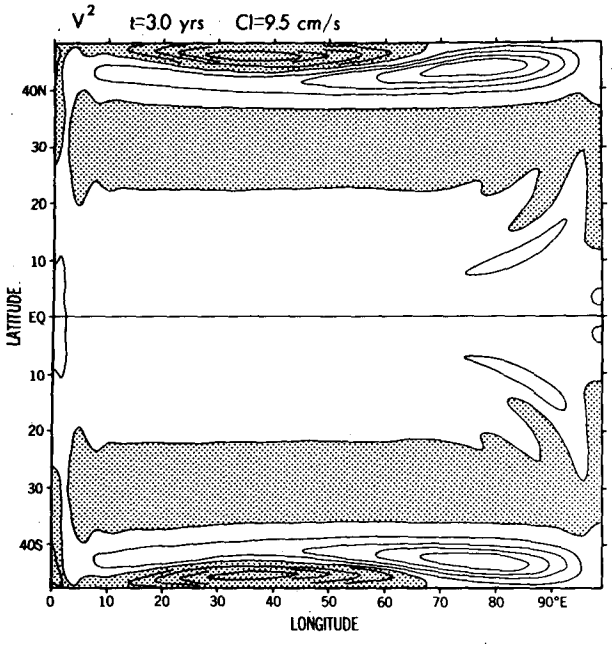

FIG. 3.4. Meridional velocity field for second baroclinic mode solutions to (3.4a–c) at t = 3.0 years.

mated to some degree by the first-mode pressure field) in equivalent regions. Meyers' region of interest was from 11 to 20°N and 40–50° west of the American coast. While noting the difference in the shape of the eastern boundary, it seems as though the results shown in Fig. 3.1a would indicate that the planetary waves might be expected to have some influence on Meyers' data.

In this regard, it should be noted that Meyers' use of a succession of Sverdrup steady states to model the geostrophic flow is incorrect, as pointed out by White (1977). The changes in the geostrophic response are affected by the planetary waves, which take several months to propagate to the region of interest. The agreement between the observations and the theoretical result is probably due to the strong influence of the Ekman flow.

a. Comparison with Oort and Vonder Haar (1976)

If the Ekman effect is indeed the single most important part of the global heat transport, Hellerman's global wind data could be used to compute heat transports for comparison with Oort and Vonder Haar (1976). Unfortunately, the existence of winds parallel to coasts will introduce another uncertainty, that of locally generated boundary currents. Using Ekman flow alone will cause high levels of convergence or divergence at the coasts, and it is not immediately obvious how much of this effect will be balanced by upwelling or by generation of boundary currents. The heat balance would be greatly affected if one were to choose one type of motion over the other. Future work will undertake to examine this question. It is noted, however, that on the basis of heat transport per unit of longitude, the Ekman model is producing an annual cycle of cross-equatorial heat transport comparable to Oort and Vonder Haar's (1976) estimate: 1.4 $\times 10^{13}$ W per degree of longitude for the Ekman cycle, 1.25 $\times 10^{13}$ W per degree of longitude from Oort and Vonder Haar's Table 12.

Oort and Vonder Haar's study is able to shed some more light on the appropriateness of the above model. The Ekman model maintains that 1) Ekman divergence accounts for most of the heat transport cycle near the equator; 2) the Ekman transport of heat is a process which puts the convergence of transport directly into storage; and 3) the surface flux/storage interaction (one-dimensional mixed layers) can be ignored because it is either small or out of phase with the transport cycle. By examining Oort and Vonder Haar's Table 11, the validity of the last two assertions can be tested.

To approach these questions, consider the complex amplitudes of the annual and semi-annual cycles of the surface flux (F_{BA}), rate of storage (S_0) and divergence of transport (divT_0). They may be represented by

$$F^n_{BA}(t) = \tilde{F}^n_{BA} e^{i\omega_n t}, \tag{4.1}$$

$$S^n_0(t) = \tilde{S}^n_0 e^{i\omega_n t}, \tag{4.2}$$

$$\mathrm{div}T^n_0(t) = \widetilde{\mathrm{div}T^n_0} e^{i\omega_n t}, \tag{4.3}$$

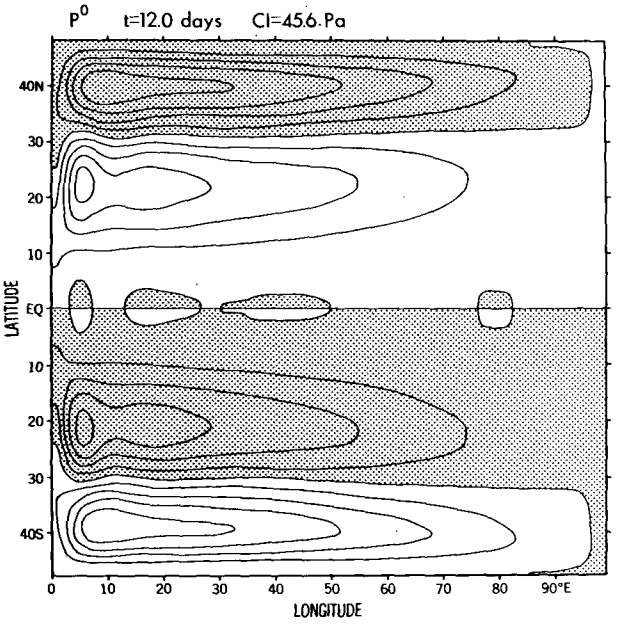

FIG. 3.5. Pressure field for the barotropic mode solutions at t = 12.0 days.

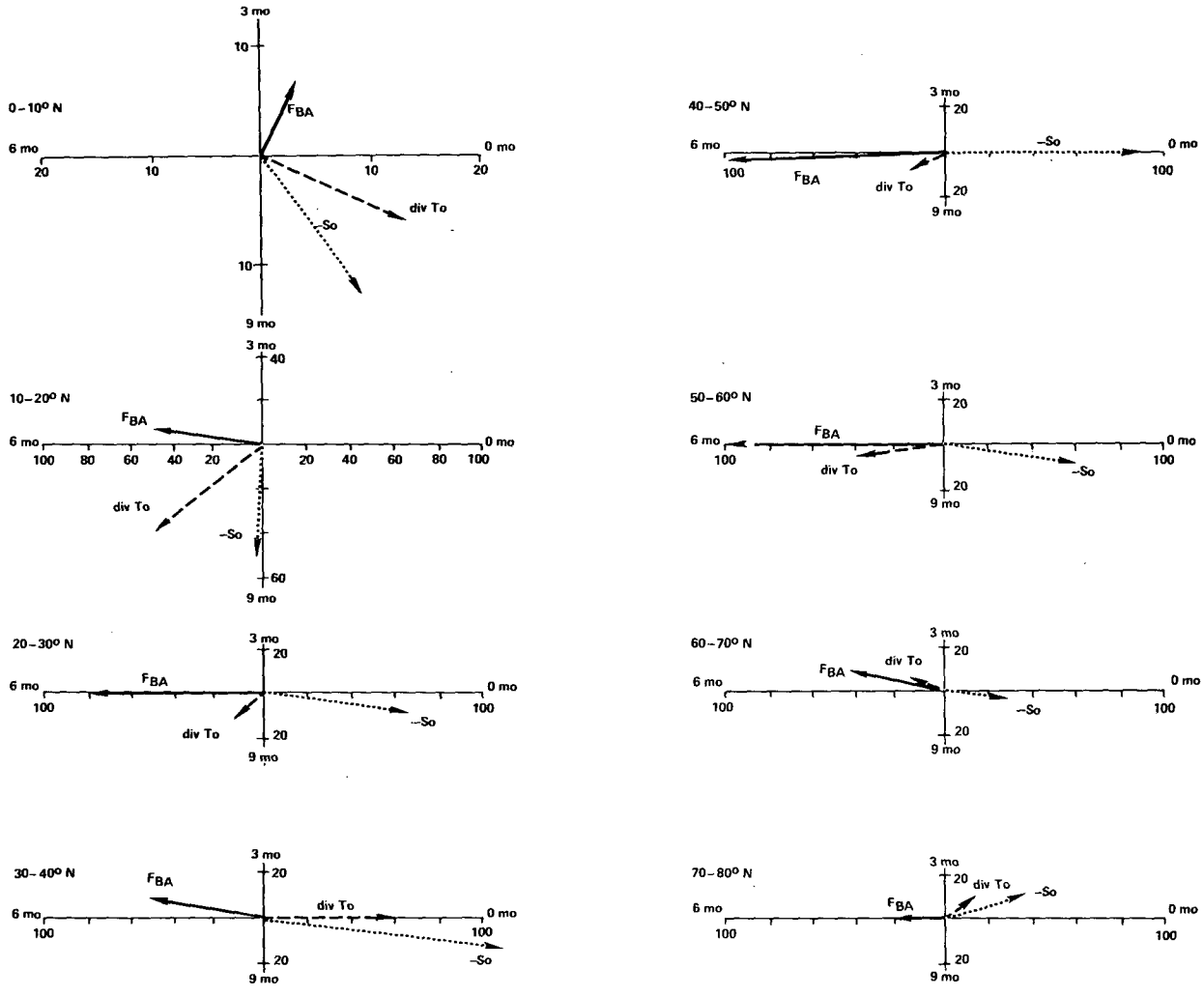

FIG. 4.1. Complex amplitudes of the annual cycles of F_{BA}, $-S_0$ and $\mathrm{div}T_0$ from Oort and Vonder Haar (1976). Note the different scale for the 0–10° latitude belt.

where $n = 1$ refers to the annual cycle, $n = 2$ to the semiannual.

The components $\tilde{F}_{BA}$, $-\tilde{S}_0$ and $\widetilde{\mathrm{div}T_0}$ are shown on the complex plane in Figs. 4.1 and 4.2 for the annual and semiannual cycles. The relative projection of $\tilde{F}_{BA}$ on $\widetilde{\mathrm{div}T_0}$ is

$$R = \mathrm{Re}\{\tilde{F}_{BA}\cdot\widetilde{\mathrm{div}T_0}^*/|\widetilde{\mathrm{div}T_0}|^2\}, \qquad (4.4)$$

where the asterisk denotes the complex conjugate. This gives the fractional amount of the divergence of transport which is crossing the surface, i.e., that amount of the transport which is not obeying the adiabatic advection mechanism used in the Ekman model. The projection of $\tilde{F}_{BA}$ on the normal to $\widetilde{\mathrm{div}T_0}$

$$I = \mathrm{Im}\{\tilde{F}_{BA}\cdot\widetilde{\mathrm{div}T_0}^*/|\widetilde{\mathrm{div}T_0}|^2\} \qquad (4.5)$$

gives the relative amount of a surface flux/storage cycle occurring out of phase with the transport. Table 4.1 lists R and I for the annual and semiannual cycles.

Note that for the annual cycle:

1) In the 0–10° band, the divergence of transport is going almost entirely into storage. This behavior is essentially similar to the mechanism proposed in the Ekman model above. In addition, however, there is a cycle in the surface flux, ~90° out of phase with the transport cycle. Its strength is about one-half of that of the transport cycle.

2) From 10 to 20°, about half of the heat accumulated by advection is stored, while half is given up to the atmosphere. A comparable one-dimensional flux/storage cycle is also occurring out of phase with

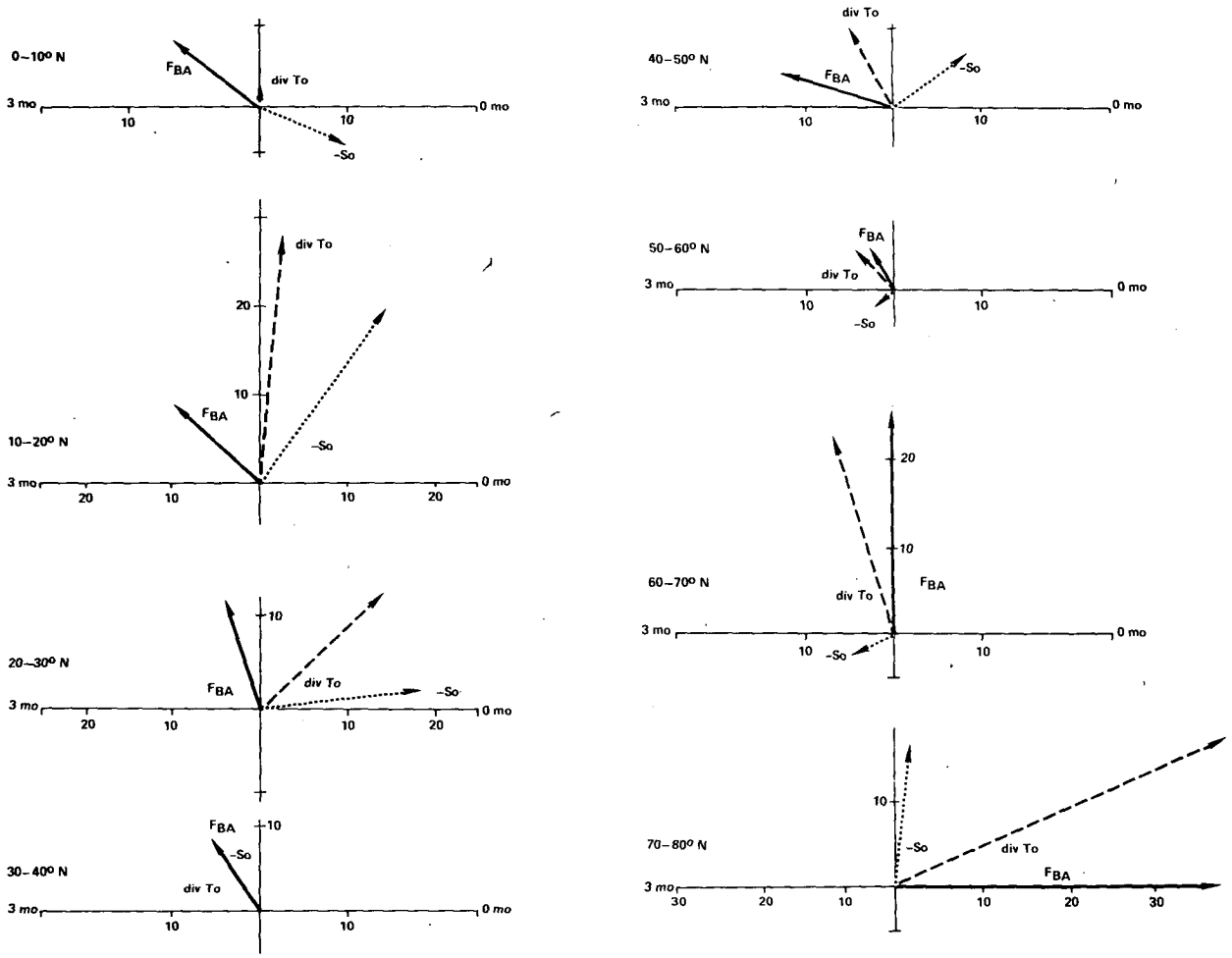

FIG. 4.2. Complex amplitudes of the semi-annual cycles of F_{BA}, $-S_0$ and divT_0 (from Oort and Vonder Haar, 1976).

the transport. Here the Ekman model is beginning to break down.

3) North of 20°, the predominant balance is between surface flux and storage, with the divergence of transport cycle having one-quarter to one-half the amplitude of this flux/storage. Here the results of the adiabatic advection model can not be expected to properly simulate the ocean.

TABLE 4.1. Normalized projections of F_{BA} on divT_0. Values determined from Oort and Vonder Haar (1976). For definition of R and I, see text.

Latitude (°N)	Annual cycle		Semiannual cycle	
	R	I	R	I
80–90	1.0	−0.5	0.5	−0.2
70–80	1.4	0.6	0.8	−0.3
60–70	−2.6	0.4	1.0	−0.3
50–60	−2.4	−0.4	0.9	−0.3
40–50	−5.3	−2.5	0.9	0.9
30–40	0.8	0.2	1.0	0.0
20–30	−3.6	−2.9	0.2	0.6
10–20	0.5	−0.6	0.3	0.4
0–10	0.0	0.6	−3.2	5.0

For the semi-annual cycle:

1) The cycles are generally smaller than their annual counterparts.

2) From 0° to 10°, $\widetilde{\text{div}T_0}$ is very small, causing large values of R and I.

3) From 10° to 30°, the adiabatic advection cycle is maintained, together with a moderate flux/storage cycle out of phase.

4) North of 30°, there is a diabatic advection mechanism, with the storage out of phase with the transport.

b. Zonally uniform winds

This study has used winds which were zonally uniform. Since they represent an average value of the zonal stress, the average Ekman transport should be closely correlated with this wind stress value. However, zonal inhomogeneities may excite Rossby waves of a different character than those included

in the finite-difference study. While this effect should be examined, it is felt that such stresses would excite waves of shorter wavelength and slower propagation speed. Therefore, they are probably less effective than the long waves in effecting zonal mean heat transport.

This assumption breaks down most importantly in coastal regions, where—as noted above—the waves and Ekman flow may interact to produce extra upwelling or coastal jets.

c. Linearized vertical temperature structure

This model advects heat by carrying a thermal field which is dependent only on the vertical coordinate. While the surface temperature of the upper ocean can vary over the seasons, in the area of interest (below 20°), the surface temperature is observed to be quite uniform. The difference between the surface temperature and the mean temperature of the deep return flow is on the order of 20°C. Variations in this difference about the year are on the order of 10% in the equatorial oceans, and should not introduce any major error in the Ekman transport estimate above.

d. Symmetric zonal wind stress components.

The analysis for the Ekman layer involved the assumption that the annual cycle in zonal stress was antisymmetric about the equator. Relaxing this condition should not lead to serious differences for the overall meridional circulation, primarily because the stress field reported by Hellerman was very close to antisymmetric. Therefore, outside of an equatorial band (scaled by the equatorial radius of deformation), the solutions should be close to Ekman, and the Ekman solution should be close to that calculated above.

The essential difference associated with symmetric zonal winds involves the increased upwelling associated with the Yoshida jet. This effect is contained within $y = 2\beta^{1/2}(gh)^{1/4}$ about the equator (6.8° for the first baroclinic mode). In the linearized model this involves a redistribution of the heat transport on each side of the equator. The effect of symmetric winds on the cross-equatorial heat transport cannot be fully determined, therefore, without the inclusion of nonlinear momentum and thermodynamic equations.

5. Summary

The annual cycle of ocean heat transport across the equator has been examined with a very simple adiabatic Ekman drift model, as well as with a slightly more complex numerical model including linear Rossby-gravity waves and friction. Employing zonally uniform, time-varying winds, it was found that the Ekman drift can produce substantial cross-equatorial heat transports, with values comparable to those estimated by Oort and Vonder Haar (1976). The presence of higher order wave dynamics did not change this response to any significant extent.

Support for an advection mechanism for heat transport was found at low latitudes from the estimates of Oort and Vonder Haar (1976). It seems clear, however, that the extension of such a model to higher latitudes is inappropriate, and that surface heat fluxes must be included.

The refinement of this study is presently being done by 1) accurate solution of variations in western boundary currents with realistic geometry and wind fields; 2) addition of surface heat fluxes and mixed-layer thermodynamics; and 3) inclusion of nonlinear dynamics at the equator and along the western boundaries.

Acknowledgment. This work was carried out at Princeton University under NSF IDOE Grant OCE-74-20693 A01. Additional support for manuscript preparation was graciously provided by Brown University and the Goddard Space Flight Center, Laboratory for Atmospheric Sciences.

The author is deeply indebted to Kirk Bryan and Abraham Oort, who provided stimulating advice and encouragement during this study. Thanks also go to S. Manabe, G. Philander and K. Deffeys for reading an earlier version of this work.

REFERENCES

Anderson, D. L. T., and A. E. Gill, 1975: Spin-up of a stratified ocean, with applications to upwelling. *Deep-Sea Res.*, **22**, 583–596.

Bryan, K., 1962: Measurements of meridional heat transport by ocean currents. *J. Geophys. Res.*, **67**, 3403–3414.

Cane, M. A., and E. S. Sarachik, 1976: Forced baroclinic ocean motions: I. The linear equatorial unbounded case. *J. Mar. Res.*, **34**, 629–665.

——, and ——, 1977: Forced baroclinic ocean motions: II. The linear equatorial bounded case. *J. Mar. Res.*, **35**, 395–432.

Levitus, S., and A. H. Oort, 1977: Global analysis of oceanographic data. *Bull. Amer. Meteor. Soc.*, **58**, 1270–1284.

McCreary, J., 1976: Eastern tropical ocean response to changing wind systems: with application to El Niño. *J. Phys. Oceanogr.*, **6**, 632–645.

Meyers, G., 1975: Seasonal variation in transport of the Pacific North Equatorial Current relative to the wind field. *J. Phys. Oceanogr.*, **5**, 442–444.

Moore, D. W., and S. G. H. Philander, 1977: Modeling of the tropical ocean. *The Sea*, Vol. 6, E. D. Goldberg, I. N. McCave, J. J. O'Brien and J. H. Steele, Eds., Wiley, 319–361.

Oort, A. H., and T. H. Vonder Haar, 1976: On the observed annual cycle in the ocean-atmosphere heat balance over the Northern Hemisphere. *J. Phys. Oceanogr.*, **6**, 781–800.

Schopf, P. S., D. L. T. Anderson and R. Smith, 1980: Beta-dispersion of low frequency Rossby waves. Submitted to *Dyn. Atmos. Ocean.*

White, W. B., 1977: Annual forcing of baroclinic long waves in the tropical North Pacific Ocean. *J. Phys. Oceanogr.*, **7**, 50–61.